Available online at www.sciencedirect.com
SCIENCE DIRECT
Polymer 46 (2005) 9396–9403
polymer
www.elsevier.com/locate/polymer

Gas foaming of segmented poly(ester amide) films

P.A.M. Lips[a], I.W. Velthoen[a], P.J. Dijkstra[a], M. Wessling[b], J. Feijen[a,*]

[a]*Institute for Biomedical Technology (BMTI) and Department of Polymer Chemistry and Biomaterials, Faculty of Science and Technology, University of Twente, P.O. Box 217, Drienerlolaan 5, 7500 AE Enschede, The Netherlands*
[b]*Membrane Technology Group, Faculty of Science and Technology, University of Twente, P.O. Box 217, 7500 AE Enschede, The Netherlands*

Received 9 March 2005; received in revised form 13 July 2005; accepted 19 July 2005
Available online 24 August 2005

Abstract

Biodegradable segmented poly(ester amide)s, based on dimethyl adipate, 1,4-butanediol and *N*,*N*′-1,2-ethanediyl-bis[6-hydroxyhexanamide], with two distinct melting transitions were gas foamed using carbon dioxide (CO_2). Polymer films were saturated with CO_2 at 50 bar for 6 h after which the pressure was released. The samples were immersed in octane at the desired temperature after which foaming started immediately. Just above the lower melt transition the polymers retain adequate mechanical properties and dimensional stability, while the chain mobility increased sufficiently to nucleate and expand gas cells during the foaming process. In this way semi-crystalline poly(ester amide)s can be gas foamed below the flow temperature.

Two poly(ester amide)s with 25 mol% (PEA2,5-25) and 50 mol% (PEA2,5-50) of bisamide segment content were foamed at 70 and 105 °C, respectively. The storage modulus (G') of both pure polymers at the onset foaming temperature is 50–60 MPa. Closed-cell foams were obtained with a maximum porosity of ~90%. The average pore size of PEA2,5-25 ranges from 77 to 99 μm. In contrast, the average pore size of PEA2,5-50 is in between 2 and 4 μm and can be increased to 100 μm by lowering the CO_2 saturation pressure to 20 bar. The porosity of PEA2,5-50 foams using this saturation pressure decreased to 70%.

Keywords: Gas foaming; Poly(ester amide); Crystallinity

1. Introduction

Polyurethane (PU), polystyrene (PS) and polyvinyl chloride (PVC) are materials traditionally applied for the manufacturing of polymer foams. PU foams are prepared by in situ generation of carbon dioxide (CO_2) while PS and PVC foams are prepared using physical blowing agents like nitrogen (N_2) and CO_2. The concept of foaming using physical blowing agents is very promising because of the lack of contaminating solvents. The use of CO_2 has a number of advantages including chemical inertness, non-combustibility, natural occurrence, low cost, ready availability, environmental acceptability (no ozone depletion) and low human toxicity. Foaming of polymers with a physical blowing agent usually results in closed-cell foams, which are generally rigid and are most suitable for thermal insulation and buoyancy.

All polymer foaming techniques using physical blowing agents rely on the same principle: (1) Saturation of the polymer with a gaseous penetrant (blowing agent) at high pressure, (2) quenching of the polymer/gas mixture into a super-saturated stage either by reduced pressure or increased temperature, and (3) nucleation and growth of gas cells dispersed throughout the polymer matrix. Upon quenching of the polymer/gas mixture the solubility of the gas in the polymer decreases, which results in clustering of gas molecules in the form of nuclei. As the gas diffuses into the forming cells, the free energy of the system is lowered. The cell nucleation process is very important as it governs the cell morphology of the material and to a large extent, the properties of the material. This process can occur homogeneously throughout the material or heterogeneously at high-energy regions such as phase boundaries. In such regions the free energy necessary to nucleate a stable void is less compared to homogeneous nucleation, resulting in preferential nucleation of voids at the interface. In semi-crystalline polymers the crystalline domains may serve as

* Corresponding author. Tel.: +31 53 489 2976; fax: +31 53 489 3823.
E-mail address: j.feijen@utwente.nl (J. Feijen).

0032-3861/$ - see front matter © 2005 Elsevier Ltd. All rights reserved.
doi:10.1016/j.polymer.2005.07.052

heterogeneous nucleation points to generate gas bubbles [1–7]. In general, cell growth is controlled by the time allowed for the gas to diffuse into the cells before quenching, the temperature of the system, the degree of supersaturation, the rate of gas diffusion into the cells, the hydrostatic pressure or stress applied to the polymer matrix, the interfacial energy and the visco-elastic properties of the polymer/gas mixture [3–5]. The stiffness of the polymer is typically controlled by the foaming temperature and a reduction in average cell size is observed at increasing stiffness [3]. The work necessary to expand the gas cell must overcome the additional stress resulting from the increased stiffness. By increasing the saturation pressure the free energy barrier for the formation of stable nuclei is decreased and additional nucleation sites are formed due to matrix swelling, free volume changes, and/or the formation of crystalline interfaces. This results in an increased cell density and consequently a decreased average cell diameter [3,4,6,8].

It is generally accepted that the sorption of gases by semi-crystalline polymers occurs exclusively in the amorphous regions [9]. The crystalline regions act as impermeable barriers due to the tight packing of the polymer chains. Many polymers do show a substantial sorption (solubility) of gas, which leads to a dramatic decrease in glass transition temperature (T_g) of these materials (plasticization), even at modest pressures [10]. Sorption of CO_2 can induce crystallization in polymers and occurs when the rate of polymer chain-segment motions makes crystallization kinetically feasible through the realignment of the chains [3,11,12].

In recent years, micro-cellular foams using CO_2 have been prepared from amorphous as well as semi-crystalline polymers [1–6,8,13–17]. A micro-cellular foam has closed-cells with an average cell sizes smaller than 10 μm and can be applied in food packaging, construction and as insulation materials [18]. Micro cellular processing follows the same foam formation mechanism as conventional prepared foams using a physical blowing agent. Semi-crystalline polymers like polypropylene (PP) [2,19,20], polyethylene terephthalate (PET) [2–5], high-density polyethylene (HDPE) [2] and polybutylene (PB) [2] have been processed into micro-cellular foams below their melting temperature. Semi-crystalline polymers exhibited considerably higher cell densities than amorphous polymers, which are attributed to a significant contribution of heterogeneous nucleation at the amorphous/crystalline interfacial regions. Since the gas does not dissolve in crystallites, the nucleation is non-homogeneous which makes it difficult to control the cellular structure of semi-crystalline foams. Polymers with a low crystallinity afforded foams with an almost uniform structure. When the crystallinity was increased, non-uniform foams with irregular cell sizes were obtained. No foaming was observed for highly crystalline polymers [2–5].

Foaming using physical blowing agents is thus a versatile technique to prepare closed-cell polymer foams. Amorphous as well as semi-crystalline polymers can be processed at a range of temperatures close to T_g up to temperatures just below the melting of the material.

Previous research showed that the incorporation of symmetrical bisamide-diol monomers into the backbone of biodegradable polyesters enhanced the thermal and mechanical properties of these materials [21–33]. These poly(ester amide)s have a micro-phase separated structure with an amide-rich hard phase and an ester-rich flexible soft phase. Depending on the amount of hard segment incorporated these aliphatic poly(ester amide)s have, besides a T_g below room temperature, a lower melt transition in between 50 and 80 °C and a higher melt transition which increased with increasing hard segment content up to 140 °C [21,25,26]. These materials are biodegradable, have thermal, physical and mechanical properties that can be tuned and have potential in foam applications. In this paper the preparation of closed-cell poly(ester amide) foams well below the highest melting temperature is described [6]. The porosity and pore size of the foams were determined as a function of foaming temperature and CO_2 saturation pressure. The relation between the thermal and mechanical properties and the foam morphology of these materials will be discussed.

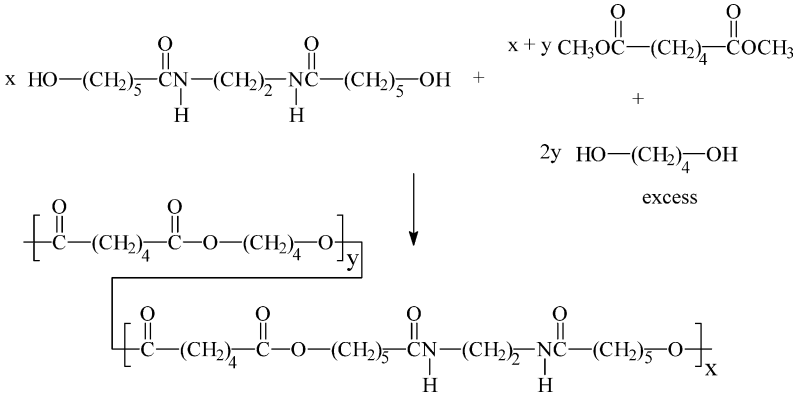

Fig. 1.

2. Experimental section

2.1. Materials

n-Octane was obtained from Merck (Darmstadt, Germany). All other solvents were obtained from Biosolve, the Netherlands. Carbon dioxide was obtained from Hoekloos (Schiedam, The Netherlands).

2.2. Polymers

2.2.1. Synthesis

A two-step polycondensation of dimethyl adipate, 1,4-butanediol and *N*,*N*′-1,2-ethanediyl-bis[6-hydroxy-hexanamide] was performed in the presence of tetrabutyl(orthotitanoate) as a catalyst, as described previously [25]. The molar ratio of hard (*x*) and soft (*y*) segments of the poly(ester amide) (Fig. 1) can be varied by changing the ratio of *N*,*N*′-1,2-ethanediyl-bis[6-hydroxy-hexanamide] and 1,4-butanediol. The polymers PEA2,5-25 and PEA2,5-50 with a hard segment content *x* of 25 and 50 mol%, respectively, were used to prepare foams.

2.2.2. Methods

The intrinsic viscosity of polymer samples was determined by a single point measurement with a capillary Ubbelohde type 0C at 25 °C, using a polymer solution with a concentration of 0.1 g dl^{-1} in chloroform–methanol (1:1 vol/vol).

Polymer films were prepared by compression moulding using a hot press (THB 008, Fontijne Holland BV, The Netherlands). Polymers were heated for 6–8 min at 20 °C above their melting temperature, pressed for 3 min at 300 kN, and cooled in approximately 5 min under pressure to room temperature.

Thermal analysis of the polymers was carried out using a Perkin–Elmer DSC-7 differential scanning calorimeter equipped with a PE7700 computer and TAS-7 software. Calibration was performed with pure indium. Measurements were performed on samples of dried polymer films after compression moulding, after CO_2 sorption (and subsequent desorption) and after gas foaming. The samples (5–10 mg) were heated from −20 to 180 °C at a rate of 20 °C min^{-1}, annealed for 5 min, cooled to −80 °C at a rate of 20 °C min^{-1}, and subsequently heated from −80 to 180 °C at a rate of 20 °C min^{-1}. Melting (T_m) and crystallization (T_c) temperatures were obtained from the peak maxima, melt (ΔH_m) and crystallization enthalpy (ΔH_c) were obtained from the area under the curve and the glass transition temperature (T_g) was taken at the inflection point. The data presented are from the second heating step, unless stated otherwise.

Differential mechanical analysis was performed with a Myrenne ATM3 torsion pendulum at a frequency of approximately 1 Hz. The storage modulus (G') and the loss modulus (G'') were measured as a function of temperature. Samples ($75\times4\times2$ mm^3) were first cooled to −100 °C and then heated at a rate of 1 °C min^{-1}. The temperature at which the loss modulus reached a maximum was taken as the T_g. The flow temperature (T_{flow}) was defined as the temperature at which the storage modulus reached 1 MPa.

The solubility of CO_2 in polymer films ($10\times4\times0.4$ mm^3), at 25 °C, as a function of CO_2 pressure (5–50 bar) was determined using a Rubotherm magnetic suspension balance operated by MessPro software. This balance has an accuracy of 1 μg. The samples were first exposed to a pressure lower than 1×10^{-4} bar, before subjecting the sample to CO_2 at the elevated pressure. The measurement was completed after a sorption plateau (constant value of the sample mass) was reached (6–8 h). The data obtained were corrected for buoyancy effects, because of the increased gas density at higher pressures.

2.3. Foams

2.3.1. Preparation

Compression moulded films ($20\times20\times0.5$ mm^3) of PEA2,5-25 or PEA2,5-50 were placed in a pressure vessel connected to a CO_2 cylinder. The samples were saturated for 6 h with CO_2 at room temperature and 50 bar. Subsequently, the pressure was quickly released and the polymer films were immersed into an octane bath, maintained at a desired temperature (40–120 °C). When visually no more gas escaped, the samples were removed from the octane bath and dried. Typical exposure times were ~1 min.

PEA2,5-50 foams were also prepared using different CO_2 saturation pressures (20–50 bar) applying the same procedure as mentioned above. Samples were subsequently immersed in an octane bath at a temperature of 105 °C.

Experiments were carried out in duplo.

2.3.2. Methods

The porosity of the gas foamed samples was determined by the flotation weight loss method, based on the Archimedes principle (ASTM D-792). The mass of a sample in air and in hexane was determined. With the known density of hexane (0.6637 g ml^{-1}) at 20 °C, the density of the sample (polymer film or foam) can be calculated according to the following equation:

$$\rho_{sample} = \frac{m}{\left(\frac{m-m_{hexane}}{\rho_{hexane}}\right)} \quad (1)$$

in which m is the mass of the dry sample in air, m_{hexane} the mass of the sample immersed in hexane and ρ_{hexane} the density of hexane. The porosity p was calculated from Eq. (2):

$$p = \left(1 - \frac{\rho_{foam}}{\rho_{unfoamed}}\right) \quad (2)$$

Scanning electron microscopy (SEM) was carried out with a LEO Gemini 1550 field emission microscope at a voltage of 2 kV. Freeze fractured samples of the porous structures were sputter-coated with gold before analysis. The average pore size and the pore size distribution were obtained by measuring the size of at least 100 pores at the cross section of the fractured foam sample.

Microcomputed tomography (μ-CT) analysis was carried out using a desktop Micro-CT 40, (Scanco Medical, Bassersdorf, Switzerland) at a resolution of 6 μm in all three spatial dimensions to provide three-dimensional reconstructions of the foam. For PEA2,5-25 foams ($0.8\times10\times10\ mm^3$), 180 slices were scanned with 1024×1024 pixels per slice. For evaluation, volumes of interest slightly smaller than the diameter of the sample were chosen to exclude crushed boundaries. The resulting gray-scale images were improved by using a low-pass filter to remove noise, and segmented with a fixed threshold to extract the polymer phase. For the 3D evaluation of the structure of the samples, 'direct' three-dimensional techniques without model-assumptions for the appearance of the structure were used. Pore voxels can be defined as voxels corresponding to the void space and polymer voxels as voxels corresponding to the polymer phase. The porosity can be calculated from the number of polymer voxels and the total number of voxels. To determine the pore sizes, pores are completely filled with modelled spheres of different diameters. The pore diameter assigned to a pore voxel is then the diameter of the largest sphere (still containing that pore voxel) that fits inside the pore [34]. In the case of non-spherical cubic pores, this method underestimates the pore size assigned to pore voxels present in the corners of these pores. Therefore, the algorithm was modified to assign the diameter of the largest sphere fitting in the pore to all pore voxels within that pore [35]. The average pore size was calculated by averaging the product of pore voxels with their assigned pore diameters over the total amount of pore voxels, according to Eq. (3):

$$\text{Average pore size} = \frac{\sum_i(\text{pore voxel}_i \times \text{pore size}_i)}{\sum_i \text{pore voxel}_i} \qquad (3)$$

3. Results and discussion

3.1. Polymer characterization

The synthesis and properties of segmented poly(ester amide)s (Fig. 1) with a hard segment content x of 25 mol% (PEA2,5-25) and 50% (PEA2,5-50), used for the preparation of foams is similar to a procedure that has previously been described [21,22,25]. These aliphatic copolymers show structural organisation through hydrogen bonding by incorporation of symmetrical rigid amide segments. The induced phase separation between the different chemical blocks leads to polymers with a glass transition temperature (T_g) below room temperature and a melting temperature (T_m) dependent on the hard segment content. The thermal and dynamic mechanical properties of these block copolymers are summarized in Table 1.

3.2. Sorption

Sorption of CO_2 in poly(ester amide) films was measured at different CO_2 pressures (Fig. 2). At all pressures PEA2,5-50 has a lower CO_2 sorption compared to PEA2,5-25, which is in line with the higher crystallinity of PEA2,5-50 (Table 1). For PEA2,5-25 and PEA2,5-50 a linear relationship between the applied CO_2 pressure and CO_2 sorption is found. CO_2 sorption may induce crystallization in the poly(ester amide)s due to enhanced mobility of the polymer chains and reorganization into a more favourable state [11]. DSC measurements revealed no change in melting temperature and enthalpy after CO_2 sorption and subsequent desorption of CO_2.

3.3. Foams

3.3.1. Foaming at different temperatures

Polymer films of PEA2,5-25 and PEA2,5-50 were saturated for 6 h with CO_2 at room temperature and 50 bar. This pressure was applied in the foaming experiments to give a maximal CO_2 sorption. When the pressure was released and the samples were immersed in an octane bath, kept at the appropriate temperature, foaming started immediately. The porosity (Fig. 3) and average pore size (Table 2) of the foams were determined as a function of foaming temperature (T_{foam}).

Table 1
Thermal and physical properties of PEA2,5-25 and PEA2,5-50 [25]

Polymer code	$[\eta]$[a] (dl g^{-1})	T_g[b] (°C)	$T_{m,1}$[c] (°C)	$\Delta H_{m,1}$[c] (J g^{-1})	$T_{m,2}$[c] (°C)	$\Delta H_{m,2}$[c] (J g^{-1})	T_{flow}[b](°C)	w_c[d] (%)
PEA2,5-25	0.73	−45	48–73[e]	16	77–115[e]	14	87	12.5±2.5
PEA2,5-50	0.63	−25	52–80[e]	7	136	26	130	27.5±2.5

[a] $CHCl_3$/MeOH (1:1 vol/vol) at 25 °C.
[b] From DMA.
[c] From DSC, 2nd heating scan.
[d] Crystallinity according to amide I band in FTIR spectra.
[e] Melting range.

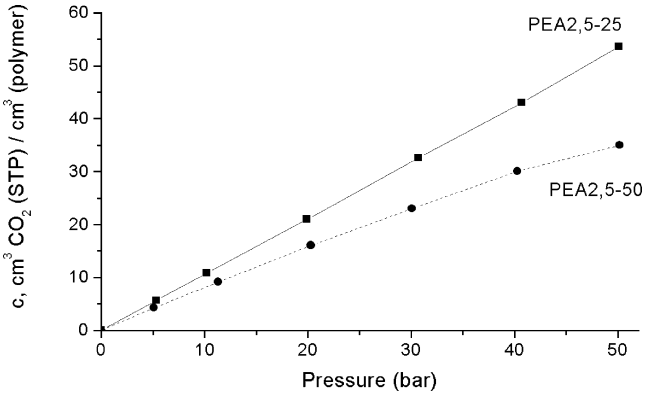

Fig. 2.

Table 2
Porosity and average pore size of PEA2,5-25 and PEA2,5-50 foamed at different temperatures (T_{foam})

Polymer code	T_{foam} (°C)	Porosity (%)	Average pore size (μm)
PEA2,5-25	60	81.6±2.6	99±42
	70	89.6±0.1	77±38
	75	89.4±1.2	87±44
PEA2,5-50	105	87.1±0.8	2.4±1.6
	110	87.2±0.7	3.8±2.5
	120	89.4±0.6	4.3±3.0

The porosity increases with increasing foaming temperature (Fig. 3). A maximum porosity of ~90% is obtained for both PEA2,5-25 and PEA2,5-50, although at a different T_{foam}. The average pore size (Table 2) and pore size distribution (Fig. 4) of PEA2,5-25 and PEA2,5-50 foams were determined. Foams with a maximum porosity of ~90% and the smallest pore size distribution are obtained at 70 °C for PEA2,5-25 and at 105 °C for PEA2,5-50, respectively. The foams have closed cells and a thin dense skin. The latter is caused by a reduced gas concentration near the polymer surface due to gas desorption during the heating step of the foaming process [6,13,36].

With micro computed tomography (μ-CT) 3D images of PEA2,5-25 foamed at 70 °C were generated. Porosity and

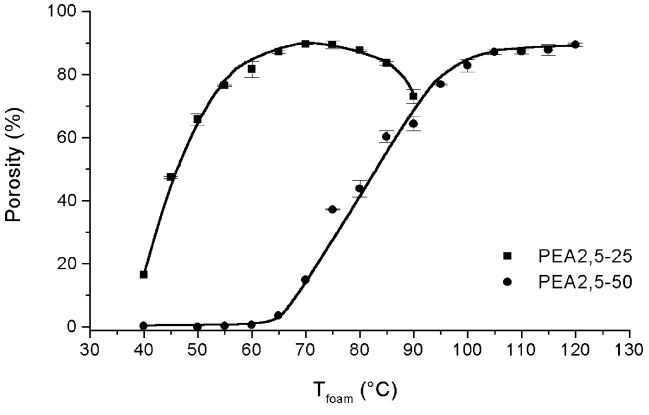

Fig. 3.

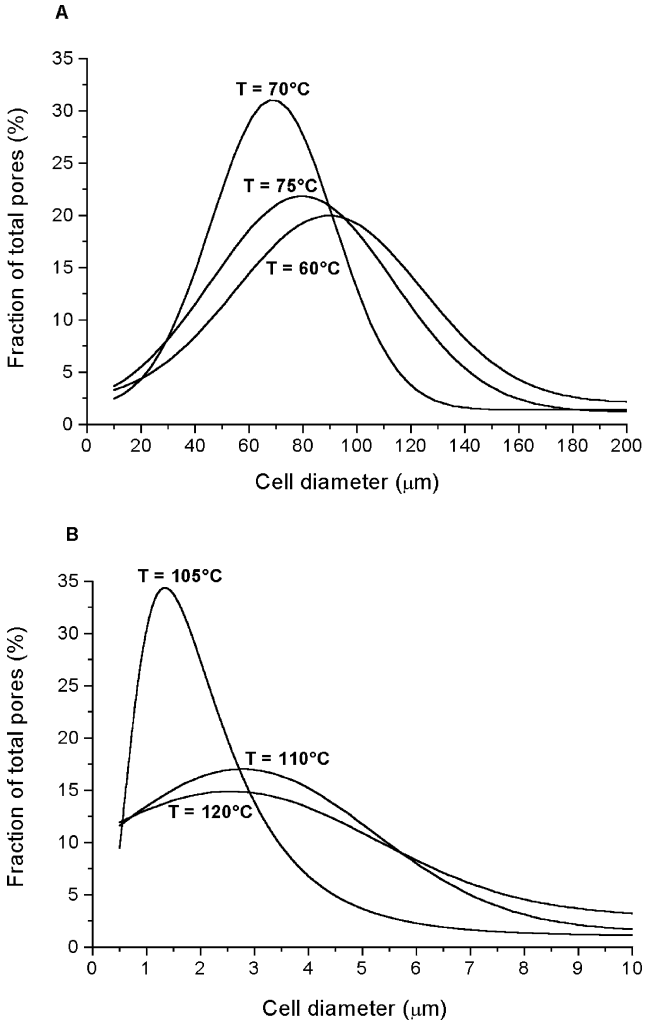

Fig. 4.

average pore size were calculated with an algorithm for cubic like pores although the pores are 'honeycomb' shaped. The porosity and average pore size obtained are 87.1% and 89 μm, respectively. The porosity is comparable to that measured by the flotation weight loss method (89.6%), whereas the average pore size is higher compared to that measured with SEM (77±38 μm). Because the thickness of the cell walls is smaller than the resolution of the μ-CT scanner (6 μm), higher pore sizes are generally determined. The pore size distribution was also determined by μ-CT and corresponds with that obtained from SEM pictures (Fig. 5). As the pores of the PEA2,5-50 foams were smaller than the resolution of the μ-CT scanner (6 μm), no data could be obtained.

The average pore size of PEA2,5-25 is significantly larger than that of PEA2,5-50 foams at a porosity of ~90% (Table 2 and Fig. 6). The crystalline domains in the CO_2 saturated polymers serve as heterogeneous nucleation agents to generate gas cells. These crystalline domains are in direct contact with the amorphous polymer matrix saturated with CO_2, providing a large interfacial area for

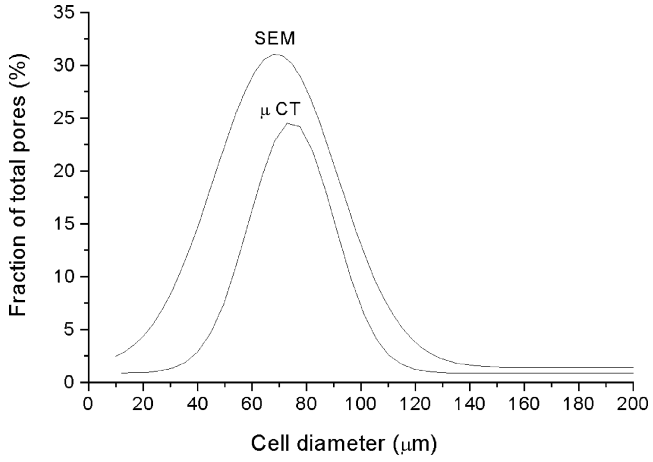

Fig. 5.

cell nucleation. Combined with a high nucleation rate this leads ultimately to a higher cell density [1–7]. When a similar amount of gas is available, more cells will nucleate in the polymer matrix with the highest crystallinity (PEA2,5-50), leading to a reduction in average pore size. Furthermore, PEA2,5-50 has a higher modulus compared to PEA2,5-25 and thus will be more difficult to expand (during cell growth) which also reduces the average pore size [3]. Thus even though the CO_2 sorption for PEA2,5-50 is lower than for PEA2,5-25 at the same CO_2 pressure, the higher crystalline PEA2,5-50 affords foams with smaller pore sizes. The pore size of the foam can thus be tuned by the hard to soft segment ratio of the polymer using similar foaming conditions.

Foaming of the poly(ester amide), which is saturated with CO_2 above its T_g, did not start before the temperature reached a critical value of 35 °C for PEA2,5-25 and 65 °C for PEA2,5-50 (Fig. 3). The driving force, which is the gas pressure gradient, below these temperatures is not high enough to overcome the attractive forces and entanglements of the polymer chains. The poly(ester amide)s show a lower melt transition ($T_{m,1}$) and a higher melt transition ($T_{m,2}$) (Table 1) [25]. It is believed that at the lower transition crystals comprising single ester amide (EA) sequences melt while at the higher transition crystals composed of 2 or more EA sequences melt. Above the lower melt transition but below the $T_{m,2}$ the polymers will retain adequate mechanical properties and dimensional stability, while the chain mobility has increased sufficiently to nucleate and expand gas cells during the foaming process. These results show that foaming of poly(ester amide)s comprising two distinct melting temperatures can be carried out well below the flow temperature. Uncontrollable cell growth, which is caused by a dramatic decrease in viscosity upon melting of the polymer is hereby prevented [19].

DMA measurements (Fig. 7) revealed a storage modulus (G') at room temperature for PEA2,5-50 of 129 MPa, which is twice as high as that for PEA2,5-25 (57 MPa). The DMA curves also reveal a transition in the rubber plateau of both poly(ester amide)s in a temperature range of 50–80 °C, similar to the $T_{m,1}$ determined with DSC (Table 1). The onset temperatures for foaming of PEA2,5-25 (35 °C) and PEA2,5-50 (65 °C) are close to these transitions. In this temperature range the storage modulus is 50–60 MPa for both pure polymers and only when the G' is lower than this value foaming can take place. Note that the plasticizing

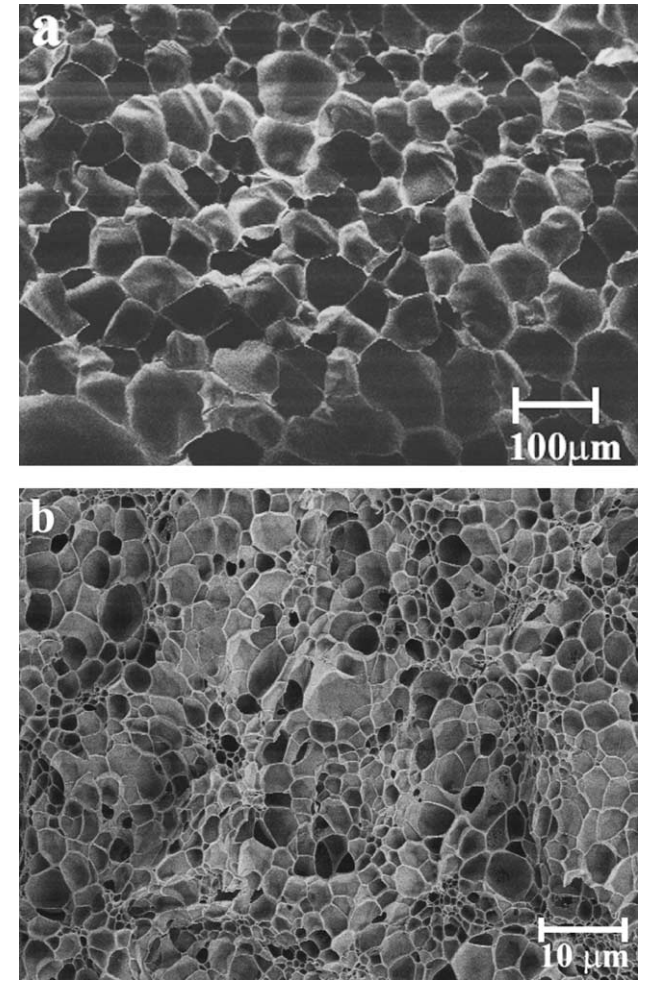

Fig. 6.

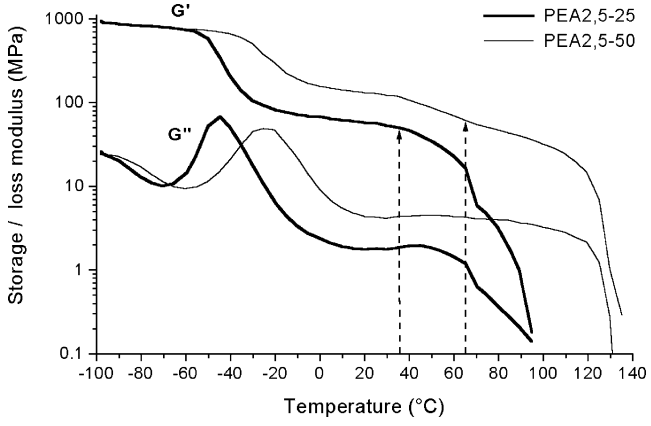

Fig. 7.

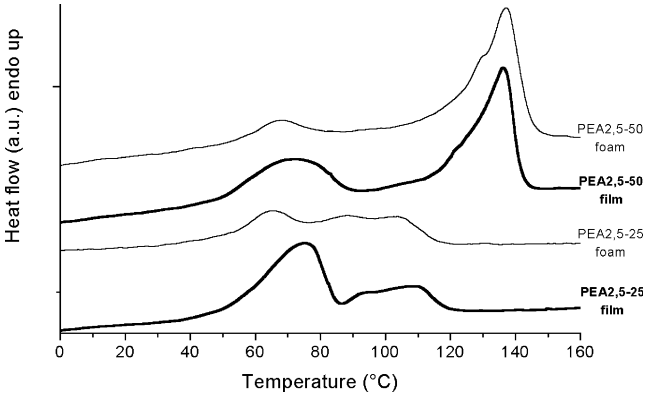

Fig. 8.

nature of CO_2 results in a shift of the storage modulus curve of the pure polymer along the temperature axis representing a depression in T_g.

No foams were obtained when the gas-saturated PEA2,5-25 and PEA2,5-50 were immersed in the heating bath with a temperature of 90 and 120 °C, respectively. As this upper foaming temperature (T_{upper}) is reached, deformation of the polymer foams is observed which was confirmed with SEM. Most likely, cells cannot grow to large sizes because CO_2 diffuses to the exterior under the strong plasticizing conditions caused by the onset of melting. The exact value of T_{upper} will depend on the melt viscosity and molecular weight of the polymer [6].

DSC measurements were performed on polymer films before and after foaming (Fig. 8). The melt enthalpy of the lower melt transition ($T_{m,1}$) of PEA2,5-50 has decreased after foaming, whereas the melt enthalpy of the higher melt transition ($T_{m,2}$) has increased. However, the total melt enthalpy has not changed, indicating that the crystal structure at the higher melting transition is more stable. Similarly the $T_{m,1}$ of PEA2,5-25 has broadened after foaming but the total melt enthalpy ($\Delta H_{m,1} + \Delta H_{m,2}$) has not changed.

3.3.2. Foaming at different saturation pressures

One way to decrease the cell density and increase the average cell diameter of the foams is to decrease the CO_2 sorption by decreasing the saturation pressure [3,4,6,8]. Polymer samples of PEA2,5-50 were subjected to different CO_2 saturation pressures and subsequently foamed at 105 °C. With increasing CO_2 concentration in the polymer the concentration of nucleation points is increased. A higher amount of gas cells will be initiated which results in smaller pores (Fig. 9). Foams with an average pore size of ~100 μm were obtained when the saturation pressure was 20 bar and an average pore size of 6 μm was obtained when the pressure was elevated to 50 bar (Table 3). Also the

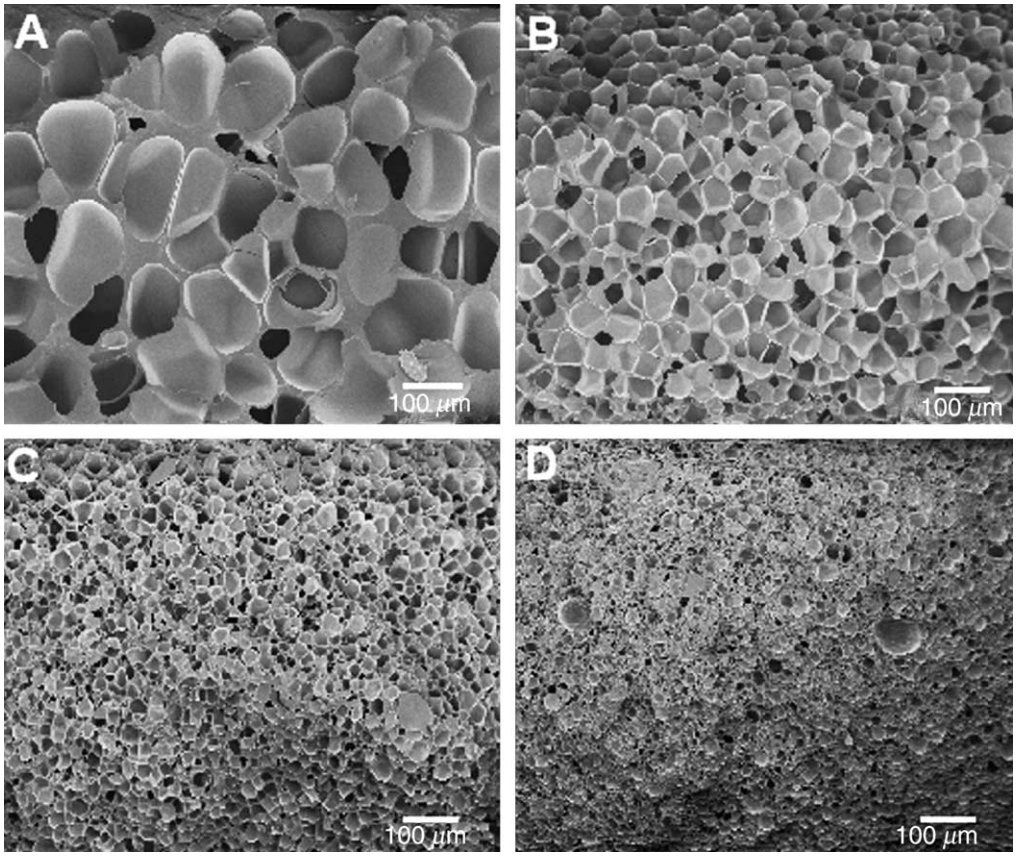

Fig. 9.

Table 3
Porosity and average pore size as a function of CO_2 saturation pressure of gas foamed PEA2,5-50 at $T_{foam} = 105$ °C

Saturation pressure (bar)	Porosity (%)	Average pore size (μm)
20	70.3±1.6	103±29
30	83.0±0.7	46±23
40	87.0±0.6	21±9
50	86.6±1.6	6±5

porosity decreased slightly with decreasing saturation pressure as at lower saturation pressures less CO_2 dissolves in the polymer. Changing the saturation pressure thus allows tuning of the average pore size of these foams.

4. Conclusions

Segmented poly(ester amide)s, comprising two melt transitions, have been gas foamed by saturation with CO_2 at elevated pressures and subsequent immersion in octane at temperatures just above the lower melt transition. At these temperatures the polymers have adequate mechanical properties and dimensional stability, while the chain mobility has increased sufficiently to nucleate and expand gas cells. The storage modulus of both pure polymers at the onset foaming temperature is 50–60 MPa. With increasing saturation pressure, the CO_2 sorption in the polymer is increasing leading to a higher concentration of nucleation points, which results in smaller pores. This study reveals that closed cell foams with a maximum porosity of ~90% and various pore sizes (2.5–100 μm) can be prepared. The pore size can be tuned by changing the saturation pressure or the bisamide to ester ratio of the poly(ester amide).

Acknowledgements

Hylke Sijbesma and Siebrand Metz (University of Twente) are acknowledged for their help with the pressure cell set up and the sorption measurements. The authors would like to thank Mark Smithers (University of Twente) for the scanning electron microscopy. Andres Laib and Markus Burkhart (Scanco Medical AG, Bassersdorf, Switzerland) are acknowledged for the micro-CT measurements. This study was financially supported by the European Commission, project: QLK5-1999-01298.

References

[1] Park CB, Baldwin DF, Suh NP. Polym Eng Sci 1995;35(5):432–40.
[2] Doroudiani S, Park CB, Korschot MT. Polym Eng Sci 1996;36(21):2645–62.
[3] Baldwin DF, Park CB, Suh NP. Polym Eng Sci 1996;36(11):1446–53.
[4] Baldwin DF, Park CB, Suh NP. Polym Eng Sci 1996;36(11):1437–45.
[5] Baldwin DF, Shimbo M, Suh NP. J Eng Mater Technol 1995;117:62–74.
[6] Krause B, Wessling M. Macromolecules 2001;34(4):874–84.
[7] Mooney DJ, Baldwin DF, Suh NP, Vacanti LP, Langer R. Biomaterials 1996;17(14):1417–22.
[8] Parks KL, Beckman EJ. Polym Eng Sci 1996;36(19):2417–31.
[9] Chen D, Hsue G. Polymer 1993;35(13):2808–14.
[10] Cooper AI. J Mater Chem 2000;10:207–34.
[11] Kazarian SG. Macromol Symp 2002;184:215–28.
[12] Shieh Y. J Appl Polym Sci 1996;59:695–705.
[13] Wessling M, Borneman Z, van den Boomgaard T, Smolders CA. J Appl Polym Sci 1994;53:1497–512.
[14] Arora KA, Lesser AJ, McCarthy TJ. Macromolecules 1998;31(14):4614–20.
[15] Krause B, van der Vegt NFA, Wessling M. Macromolecules 2001;34(25):8792–801.
[16] Doroudiani S, Park CB, Kortschot MT. Polym Eng Sci 1998;38(7):1205–15.
[17] Stafford CM, Russel TP, McCarthy TJ. Macromolecules 1999;32(22):7610–6.
[18] Klempner D, Frisch KC. Handbook of polymeric foams and foam technology. New York: Hanser; 1991.
[19] Colton JS. Mater Manuf Process 1989;4(2):253–62.
[20] Colton JS, Suh NP. Polym Eng Sci 1987;27(7):485–92.
[21] Stapert HR, Dijkstra PJ, Feijen J. Macromol Symp 1998;130:91–102.
[22] Stapert HR, Bouwens AM, Dijkstra PJ, Feijen J. Macromol Chem Phys 1999;200(8):1921–9.
[23] Sudha JD, Pillai CKS, Bera S. J Polym Mater 1996;13(4):317–28.
[24] Sudha JD. J Polym Sci, Part A: Polym Chem 2000;38:2469–86.
[25] Lips PAM, Broos R, van Heeringen MJM, Dijkstra PJ, Feijen J. Polymer 2005;46:7823–33.
[26] Lips PAM, Broos R, van Heeringen MJM, Dijkstra PJ, Feijen J. Polymer 2005;(46):7834–42.
[27] Katayama S, Murakami T. J Appl Polym Sci 1976;20:975–94.
[28] Katayama S, Horikawa H. J Appl Polym Sci 1971;15:775–96.
[29] Horton VL, Blegen PE, Barrows TH, McQuin RL. Prog Biomed Polym Los Angeles 1988.
[30] Bera S, Jedlinski Z. J Polym Sci, Part A: Polym Chem 1993;31(3):731–9.
[31] Bera S, Jedlinski Z. Polymer 1992;33(20):4331–6.
[32] Bera S, Jedlinski Z. Polymer 1993;34(16):3545–7.
[33] Barrows TH. The design and synthesis of bioabsorbable poly(ester–amides). Polymers in medicine II. New York: Plenum; 1986.
[34] Hildebrand T, Ruegsegger P. J Microsc 1997;185:67–75.
[35] Claase MB, PhD Thesis, Enschede: University of Twente: 2004.
[36] Harris LD, Kim BS, Mooney DJ. J Biomed Mater Res 1998;42(3):396–402.